Journal of Instrumentation

RaDoM: a lung dosimeter for radon progeny

Published by IOP Publishing for Sissa Medialab

Received: *February 8, 2018*
Revised: *May 31, 2018*
Accepted: *July 19, 2018*
Published: *July 30, 2018*

2018 JINST 13 P07030

RaDoM: a lung dosimeter for radon progeny

S. Romano,[c,d,1] **M. Caresana,**[a] **L. Garlati,**[a] **F. Murtas**[b,c] **and M. Silari**[c]

[a] *Politecnico of Milan,*
Piazza Leonardo da Vinci 32, Milan, Italy
[b] *INFN,*
Via Enrico Fermi 40, Frascati, Italy
[c] *CERN,*
1211 Geneva 23, Switzerland
[d] *UPC,*
Campus Nord, Calle Jordi Girona, 1–3, Barcelona, Spain

E-mail: stefano.romano@cern.ch

Abstract: This paper discusses a novel Timepix-based on-line radon dose monitor called RaDoM. The detector provides a direct estimate of the effective dose to the lung via a system of filters having the same absorption characteristics as this organ and a measurement of the PAEC (the potential alpha energy concentration). Measurements performed in a reference radon chamber and in normal environmental conditions showed that RaDoM well follows changes in the radon concentration and is accurate in both long- and short-term measurements. The paper describes the detector and associated software for data acquisition and analysis, and compares the measurement of the lung dose with the value derived from a measurement of the radon concentration.

Keywords: Detector design and construction technologies and materials; Dosimetry concepts and apparatus; Solid state detectors; Spectrometers

[1] Corresponding author.

https://doi.org/10.1088/1748-0221/13/07/P07030

Contents

1 Introduction

Radon is a radioactive gas that represents the most important source of human radiation exposure among those of natural origin [1]. Radon is chemically and electrically inert, therefore, after inhaling, is immediately exhaled. Radon is weakly harmful in itself, but the daughter products attach to ambient aerosol particles, which may be inhaled and stick to the lung surface. Among the daughter products, the most relevant ones are the alpha-emitters ^{214}Po and ^{218}Po isotopes, which cause highly localised radiation damage to cells and may lead to lung cancer. The major health concern comes from the deposition of radon progeny on the epithelial cells of the bronchial airways [2]. The choice of the radon measurement technique depends on the time over which an instrument can be devoted to a measurement at a single location, the kind of information required, the desired accuracy with which measurements can be related to an estimate of risk, and on the costs involved. Radon measurements are often discussed in terms of either short-term or long-term data acquisition. Since the radon concentration in the same location can vary due to the season, the weather conditions and the air exchange, a short-term measurement may provide only a first indication of the mean long-term concentration. Therefore, in order to assess the annual average radon concentration, devices that provide a long-term integrated measurement are preferred [3]. However, the correlation between radon concentration and effective dose is made assuming standard values of equilibrium factor ($F = 0.4$) and unattached fraction of the potential alpha energy, PAE (8%) [4]. If the conditions in the specific measurement site are far from the standard ones or are not constant over the measuring period, the simple measurement of radon concentration can lead to an overestimation or an underestimations of the effective dose. As radon concentration measurements are quite reliable, cheap and well established, they can be regarded as an important instrument for screening a huge number of sites. However, a reliable dose assessment is not possible because it requires the analysis of the size of airborne particulate and a dedicated detector to measure the equilibrium factor. To overcome the intrinsic limitation of long-term radon concentration

2018 JINST 13 P07030

measurements, as far as dose assessment is concerned, this paper discusses a novel on-line radon dose monitor (RaDoM). The detector has a response that is directly proportional to the effective dose. This result is obtained by 1) sampling air through to a system of filters having a particulate absorption characteristic that mimics the one of the extra-thoracic airways, and 2) by measuring the potential alpha energy concentration (PAEC). The RaDoM is the evolution of two radon detection systems called RADONPIX and RADONLITE developed at CERN in the past few years [5] and shares with them the Timepix hybrid silicon detector as sensor.

2 The RaDoM

RaDoM is made of a Timepix sensor (see for instance ref. [6] and references therein quoted), a system of aerosol filters and a pump for air sampling. The pump draws the air and the radon decay products through the system of filters. The Timepix counts the alpha particles from the radon daughters attached to the filter. In order to obtain a direct estimate of the effective dose, the system of filters was designed so as to have absorption characteristics similar to those of the respiratory tract. RaDoM responds well to changes in environmental conditions and is accurate in both long- and short-term measurements. Its response is not affected by natural background radiation thanks to the Timepix pattern recognition capability and to the cluster analysis algorithm developed in this work. Furthermore, RaDoM solves the ^{210}Po contamination problem, which was a major issue with RADONPIX and RADONLITE [figure 1] as well as with most commercial active radon monitors. ^{210}Po is a long-lived radon decay product with a half-life of 22 years. In RaDoM the decay products attach to the filter, which can be easily replaced, rather than to the detector surface, as it occurs in existing radon monitors.

2.1 Detector design

The working principle and the geometrical configuration of RaDoM is sketched in figure 2. The pump draws the air containing radon and the radon decay products through the system of mesh screens. Depending on the type of mesh and the chosen configuration of the system, either single or four mesh screens, it is possible to build different versions of the dosimeter. The paper filter, placed above the Timepix silicon sensor, stops the radon decay products that have not been collected by the mesh screens. The alpha particles from the radon daughters attached to the filter are then counted by the Timepix. The size distribution of the particles collected on four 400-mesh (400 holes per inch, corresponding to a wire diameter of 27 μm) screens matches the dose conversion factor (DCF) [7] curve of the tracheobronchial region, which has high susceptibility to radiation-induced cancer, with a response proportional to the effective dose. Figure 3 shows the final design of the RaDoM. The materials are PVC for the case and aluminum for the filter holder. The paper filter is a Millipore AA 0.8 μm thick, chosen for its high collection efficiency for radon progeny (99.99%) [8]. The pump is a NMP 05 M model produced by KNF in Germany [9], with maximum air volume sampling rate of 0.3 l/min. The pump is connected to the detector though the central hole in the upper side of the detector. The others holes are for the 3 mm screws used to tighten the various parts of the RaDoM together. The filter drawer (dark grey in figure 3) keeps the Millipore filter exactly aligned to the silicon sensor at a distance of 13.4 mm. Figure 4 shows the filter fixing mechanism. The holder (A) fixes the Millipore filter (B) to the drawer (C). A standard 3 mm threaded hole (D) allows to easily

2018 JINST 13 P07030

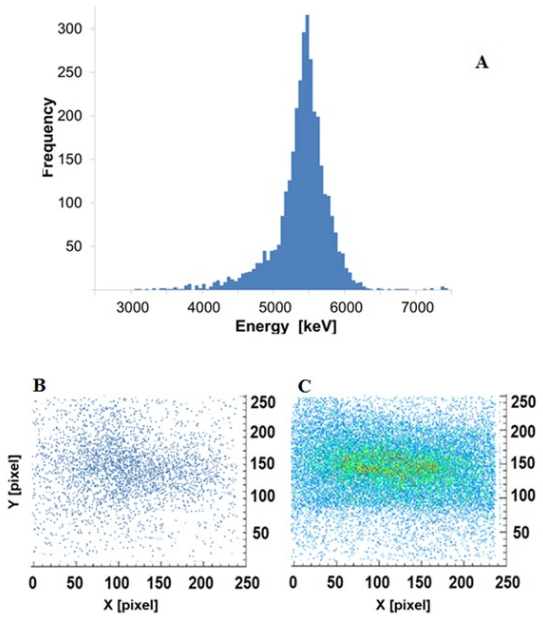

Figure 1. [A] Alpha particle energy distribution in the Timepix sensor of RADONLITE, in which the peak of the ^{210}Po at 5.3 MeV is evident. [B] Position of alpha particles from ^{210}Po on the silicon sensor one year after radon measurements [C]. Position of alpha particles from ^{218}Po on the silicon sensor during radon measurements.

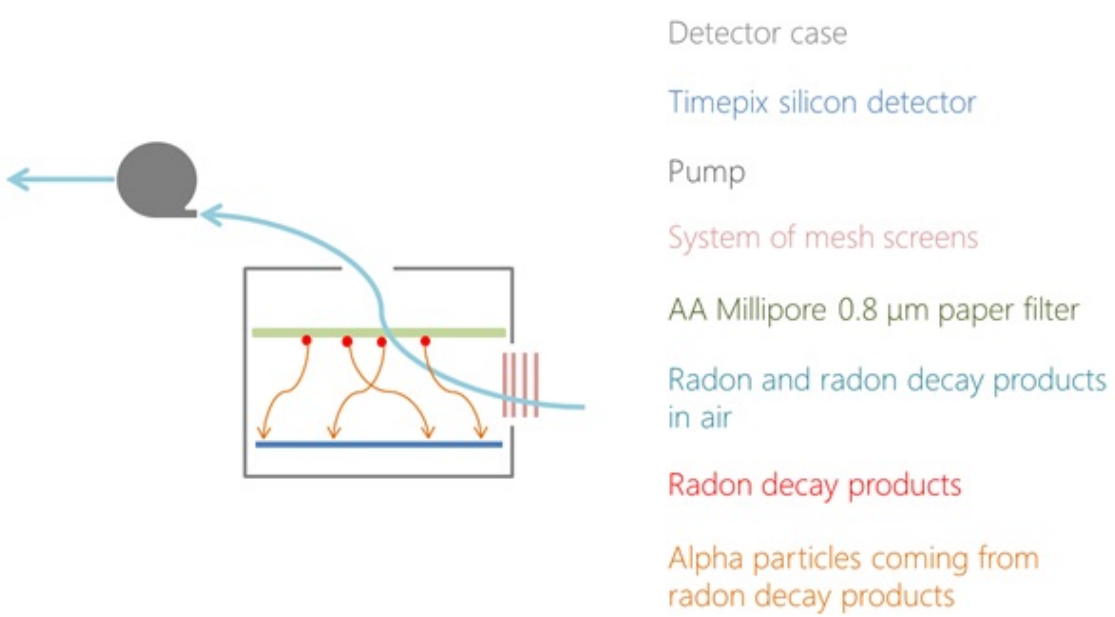

Figure 2. RaDoM schematic.

2018 JINST 13 P07030

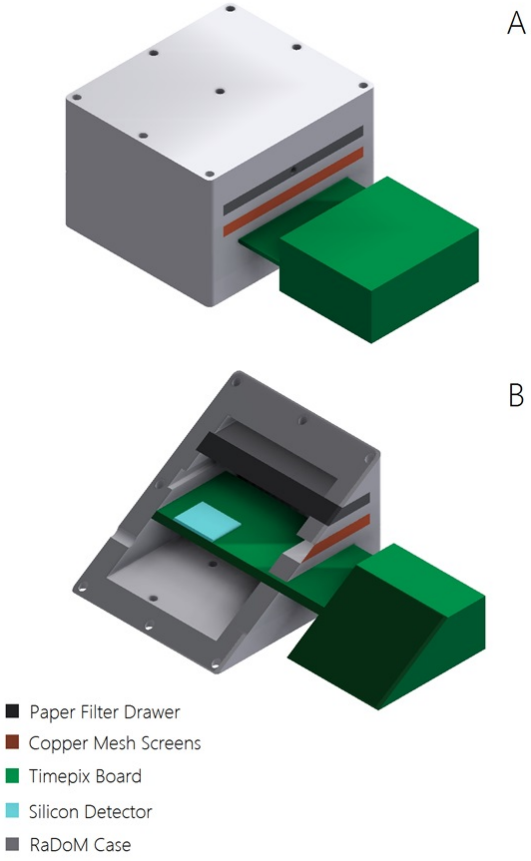

Figure 3. 3D model of RaDoM. A): assembled view; B): cross sectional view.

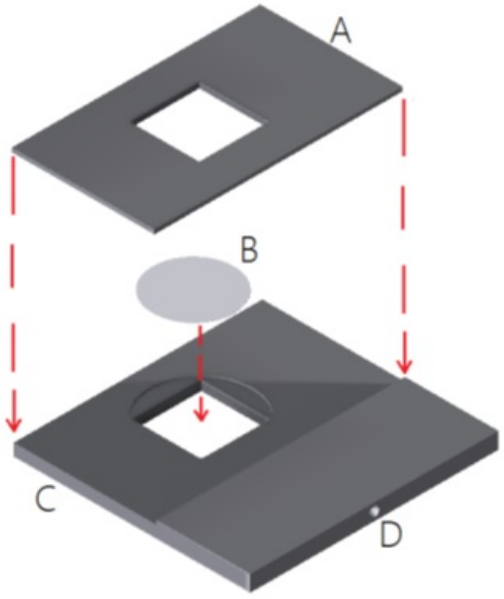

Figure 4. Filter drawer. The holder (A) fixes the Millipore filter (B) to the drawer (C). A standard 3 mm threaded hole (D) allows to easily extract the drawer from the RaDoM.

2018 JINST 13 P07030

extract the drawer from the RaDoM in order to change the filter without disassembling the detector. Figures 5 and 6 show exploded and assembled views of the detector prototype. By removing the mesh screens, RaDoM can be used as a PAEC detector, in which configuration it counts the alpha particles from the radon progeny that attached to the filter surface. Thanks to the high collection efficiency of the filter, almost all radon decay products are stopped [8] and their alpha particles counted. In radon monitoring, the potential alpha energy concentration is mostly expressed in Working Level [WL]. The WL is defined as any combination of short-lived radon products in one litre of air that will result in the ultimate emission of potential alpha particle energy equal to 1.3×10^5 MeV. In air, this energy is released when an equilibrium concentration of 3700 Bq/m^3 is present. Using expression 2.1[10], in which [^{218}Po], [^{214}Pb] and [^{214}Bi] are the concentrations of the relevant radon decay products in number of their atoms per litre, it is possible to obtain a precise estimation of the Working Level or PAEC.

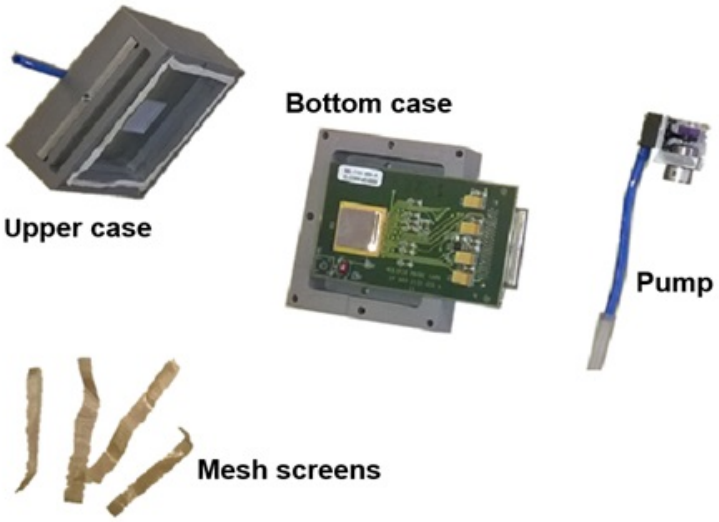

Figure 5. Exploded view of the RaDoM prototype.

$$WL = \frac{13.69[^{218}\mathrm{Po}] + 7.69\left(\left[^{214}\mathrm{Pb}\right] + \left[^{214}\mathrm{Bi}\right]\right)}{1.3 \cdot 10^5} \tag{2.1}$$

The PAE (potential alpha energy) is the total energy emitted in the alpha decay of the radionuclide to ^{210}Pb. Therefore it is 13.69 MeV (6.0 MeV+ 7.69 MeV) for ^{218}Po and 7.69 MeV for ^{214}Pb and ^{214}Bi. In the RaDoM, the Timepix counts the alpha particles coming from both ^{218}Po and its decay product ^{214}Po, because both radon daughters remain attached to the filter surface. This leads to an increase in the ^{214}Po counts. By using a value of 6.0 MeV for the PAE of ^{218}Po rather than 13.69 MeV the real value of the PAEC is obtained. The RaDoM geometrical efficiency is 15.6%, defined by the ratio between the solid angle between the filter and the silicon surface and 4π. A second prototype, which uses a quad Timepix, was also developed. The quad Timepix has four chips and $2.8 \cdot 2.8$ cm^2 active area. This prototype has a geometrical efficiency of 33.2% thanks to the larger sensor area and shorter distance between the filter and the silicon surface.

2018 JINST 13 P07030

Figure 6. Assembled view of the RaDoM prototype.

2.2 Acquisition and analysis software

In the Timepix detector, different types of ionizing radiation create different types of clusters because of their different dE/dx. Thereby by analysing specific properties of the cluster, such as its morphology or the energy released, the cluster can be classified and assigned to a specific particle category. A software code in Python language for offline analysis, PyPix, was written. A software for online analysis, RADON MONITOR, has been described in a previous paper [5]. The principle of the PyPix algorithm is as follows. A loop over the pixel matrix looks for aggregate pixels that have a much higher number of hits than the average; the found clusters are compared with the default parameters registered in the algorithm. For example, circular clusters with eccentricity up to 0.1 are classified as heavy blobs, random paths are categorized as curly tracks, linear paths as straight tracks, etc. The eccentricity is a parameter associated with a conic section. It can be thought of as a measure of how much a conic section deviates from being circular (the eccentricity of a circle is zero). Figure 7 shows a one-minute frame acquired in the radon chamber at Politecnico di Milano with the RaDoM. Dust inside the chamber has been generated by the combustion of incense. In figure 7 different kinds of tracks are distinguishable, such as heavy blobs, curly tracks, dots and straight tracks. The algorithm recognizes and categorizes the clusters. Comparing the ToT (Time over Threshold) counts (which correspond to the energy deposition if the Timepix is calibrated) and the size of the cluster with the kind of track, the algorithm assigns a specific particle to each cluster. For example, heavy charged particles lose energy in silicon according to the Bethe-Bloch equation, and therefore an alpha particle creates a heavy blob because of its short range. An electron loses its energy by collisions or by Bremsstrahlung so its path is random, and this leads to the creation of a curly track. Therefore in figure 7 cluster number 1 is a muon, cluster 2 is an alpha particle, cluster 3 is an electron and cluster 4 is a photon. In particular the overlapping alpha particle and electron (cluster 5) is due to the decay of ^{214}Po, which occurs 164 µs after the decay of ^{214}Bi producing a blob (alpha particle) with a tail (beta particle). In fact, some of the

2018 JINST 13 P07030

particles attach to the sensor surface rather than to the Millipore filter because most of the dust generated by combustion is electrically charged [11] and it is attracted by the electric field generated by the detector bias voltage.Thanks to the spectroscopic capabilities of the Timepix, the script distinguishes the alpha particles coming from ^{218}Po, ^{214}Po and ^{210}Po, and removes the background. Some examples of the PyPix interface are shown in figures 8 and 9. Figure 8 is a scatter plot of energy deposition as a function of the cluster size for all particles (A) and for alpha particles (heavy blobs) only (B): it is also possible to distinguish the two peaks due to ^{218}Po and ^{214}Po both in the energy and in the size spectra. Figure 9 shows the counts of ^{218}Po (blue) and ^{214}Po (red) as a function of time with their statistical uncertainties. WALKABOUT [12] is a python-based server

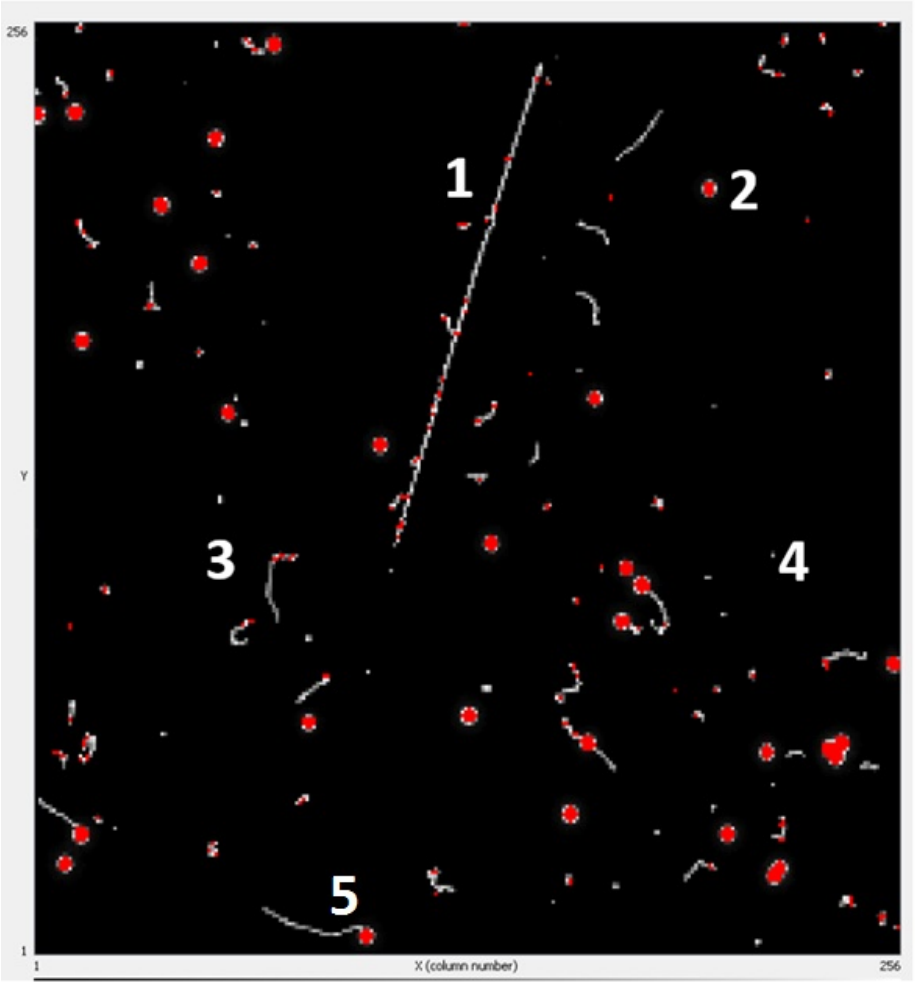

Figure 7. A one-minute frame acquired in the radon chamber at Politecnico di Milano with the RaDoM. 1: straight track. 2: heavy blob. 3: curly track. 4: dot. 5: overlapping alpha particle and electron.

we have developed, to which the RADON MONITOR plugin can be connected. The functioning principles of the server are schematized in figure 10. The RaDoM is connected by an USB cable to a computer running the Pixelman [13] software and the RADON MONITOR plugin [5]. RADON MONITOR displays the results of the measurement in real time, saves the data and sends them to the WALKABOUT server via internet, Wi-Fi or locally if the server is installed on the same computer

2018 JINST 13 P07030

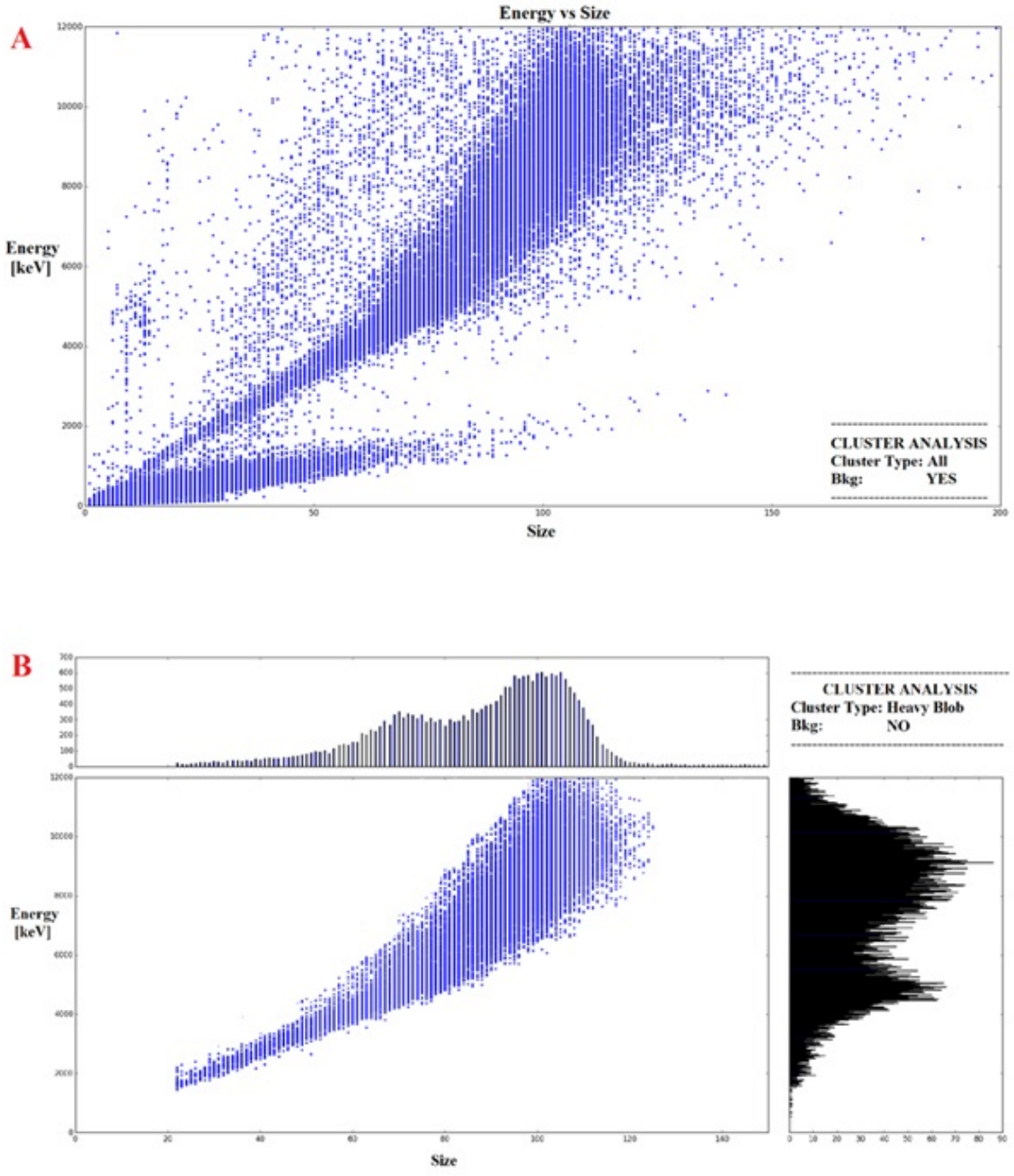

Figure 8. Scatter plot of energy deposition as a function of the cluster size for all particles (A) and for alpha particles (heavy blobs) only (B).

as the RADON MONITOR plugin. The server is a native Python integration framework. It includes several libraries for data analysis, such as Numpy, Scipy, Matplotlib [14] and Root [15], allowing to perform complicated analysis remotely by exploiting the different types of libraries without having them installed on the computer connected to RaDoM. This makes possible to use mini-computers with low processing power, in order to have a complete (sensor+computer) but small detector.

2018 JINST 13 P07030

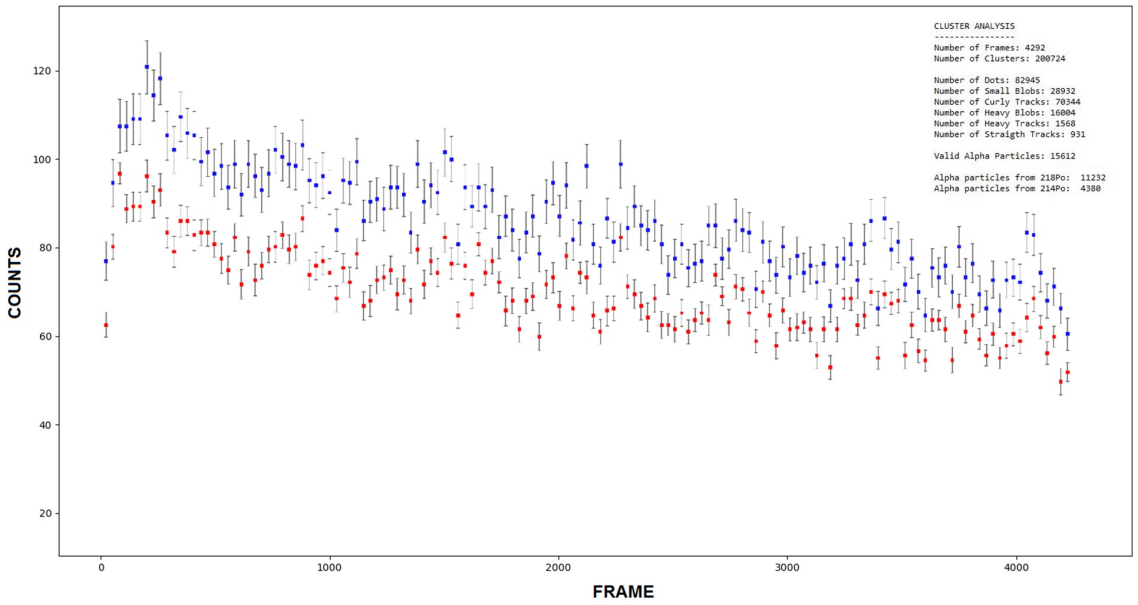

Figure 9. Counts of ^{218}Po (blue) and ^{214}Po (red) as a function of time.

Thanks to this system, it is also possible to remotely connect to WALKABOUT using portable devices, such as a smartphone or a tablet, observing the results of the measurement in real-time from anywhere (figure 10). The present results indicate that RaDoM is a good candidate for real-time radon dose monitoring, due to the features of the Timepix detector combined with a proper design of the instrument and an appropriate cluster analysis and pattern recognition algorithm. The three different software solutions, RADON MONITOR, WALKABOUT and PyPix make RaDoM user-friendly, in spite being a rather powerful and sophisticated analysis tools.

3 Measurements, results and discussion

3.1 Effective dose measurements

RaDoM in the dose configuration was first tested in the calibration laboratory of the Radiation Protection group at CERN [16], where an ambient radon concentration of about 100 Bq/m^3 is present. The duration of the measurement was 15.45 days. The configuration chosen was four copper mesh screen in series with a wire diameter of 30 µm. According to Cheung et al. [7] and Hopke et al. [17], four 400-mesh screens simulate the collection characteristic of the tracheo-bronchial region. In order to count the alpha particles from the radon decay products attached to the four 400-mesh screen, parallel measurements with two detectors are needed, as the Timepix is only able to count the alpha particles coming from the nearest mesh. Figure 11 shows the set-up of the two detectors for the simultaneous measurements. Detector A has the four 400-mesh screen whereas detector B only has the Millipore filter. The latter is RaDoM in the PAEC configuration with the quad Timepix chip. Figure 12 shows the detectors A and B during measurement in the calibration laboratory at CERN. The collection efficiency [7] of the wire screen series is obtained by expression 3.1:

2018 JINST 13 P07030

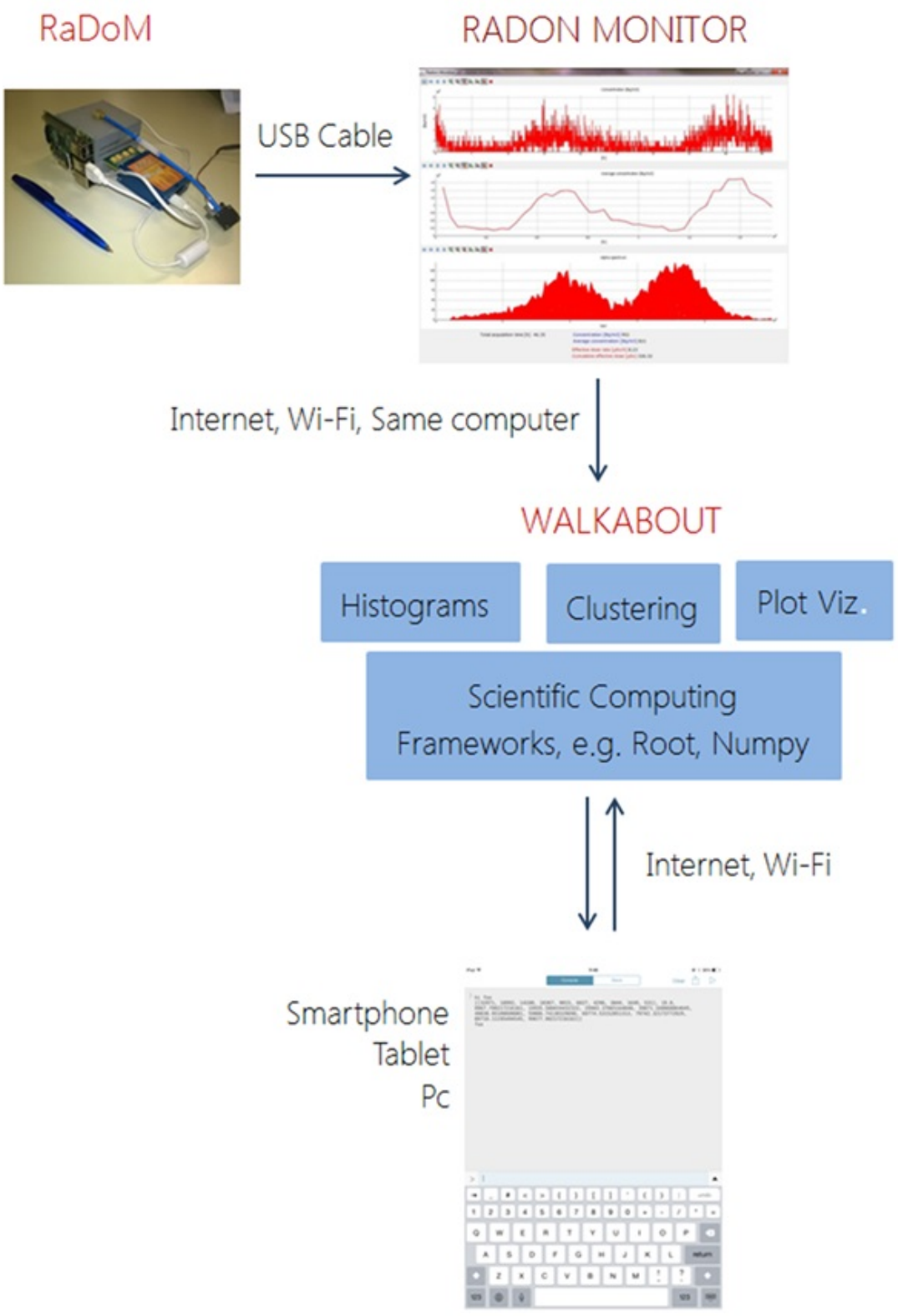

Figure 10. Functioning principle of the WALKABOUT server.

2018 JINST 13 P07030

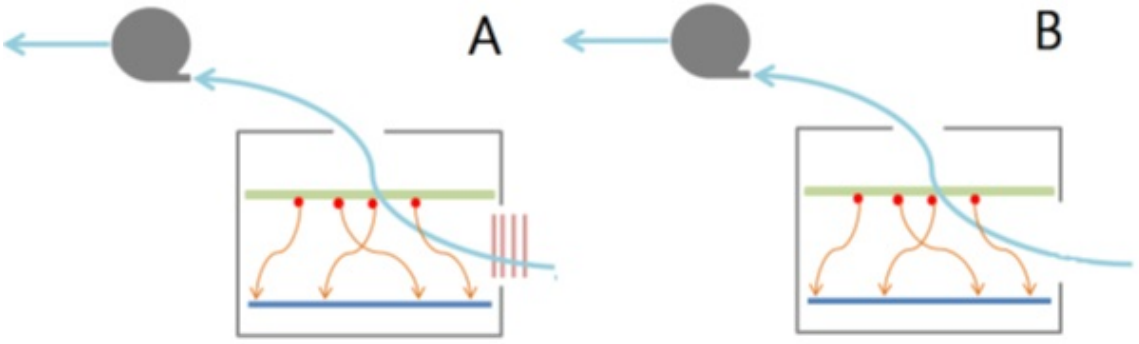

Figure 11. Set up for simultaneous measurements. A) Four mesh screens + Millipore filter. B) Millipore filter only.

Figure 12. Detectors A and B in the calibration laboratory at CERN.

$$\epsilon_{\text{wire}} = \frac{\text{PAEC}_B - \text{PAEC}_A}{\text{PAEC}_B} \tag{3.1}$$

PAEC_A and PAEC_B (in Working Level) are calculated by expression 2.1. The DCF for this configuration is $2.66 \cdot 10^{-4}$ mSv/(s·WL) [7]. Therefore the effective dose is obtained by expression 3.2, where t is the duration of the measurement in seconds and $\epsilon_{\text{geometry}}$ the geometrical efficiency of the detector. The integrated effective dose over the 15.45 days of exposure is 0.0283 ± 2.3% mSv.

$$\text{Dose} = \frac{\text{DCF} \cdot \epsilon_{\text{wire}} \cdot \text{PAEC}_B \cdot t}{\epsilon_{\text{geometry}}} \tag{3.2}$$

The uncertainty is assessed composing: (a) the statistical uncertainty supposed Poisson distributed (Type A), (b) the systematic (Type B) uncertainty in the collection efficiency on the wire mesh

2018 JINST 13 P07030

screen (12.4%) and (c) the systematic (Type B) uncertainty associated to the unattached fraction of PAEC (8%) [7]. Since the two systematic uncertainties are not correlated, the overall systematic uncertainty is 14.7% (quadratic sum of uncertainties). The effective dose calculated from the radon concentration is 0.0278 ± 0.0018 mSv assuming an indoor occupancy factor of 0.2 (workplace) and an equilibrium factor of 0.4 (dwellings). The effective dose was calculated by using the value of the committed effective dose rate E [4, 18], expression 3.3, multiplied by the exposure time.

$$E = C_{\mathrm{Rn}} \cdot D \cdot F \cdot T \cdot W_R \cdot W_T \tag{3.3}$$

Here C_{Rn} is the radon concentration expressed in Bq/m^3, D is the conversion factor equal to $9.0 \cdot 10^{-6}$ mGy/h per Bq/m^3 [4], F is the equilibrium factor equal to 0.4 (indoor radon), T is the indoor occupancy factor equal to 0.2 for workplaces (2000 h/y) or 0.8 (7000 h/y) for domestic places, $W_R = 20$ and $W_T = 0.12$ [19] are the radiation weighting factor for alpha particles and the tissue weighting factor for lung, respectively. The result of the present measurement is in good agreement with the value calculated from the radon concentration (the standard method).

3.2 Test in radon chamber

Inside the radon chamber the effective dose is generally lower than in a real environment for the same concentration. This is because of two phenomena. First, the value of the equilibrium factor is much lower than 0.4 due to the small volume of the chamber (1 m^3) and because the radon progenies tend to stick to the walls of the chamber rather than lingering in the air. Second, the air inside the chamber is filtered twice, so it is dust-free. For these reasons the radon chamber is not the ideal place to test the RaDoM, since the chamber lacks a "dust generator". In order to generate particulate, incense was burnt inside the chamber. This certainly cannot give precise information on the capability of RaDoM to determine the dose, because the generated dust is very different from the particulate found in a normal environment. However this test was useful to understand the response of the detector to changes in the amount of dust. Figure 13 shows the measurement set-up. Figure 14 shows the effective dose rate estimated directly with the RaDoM and calculated from the radon concentration assuming the standard equilibrium factor of 0.4. As soon as incense started to burn, the counts of the radon decay products started to increase. After 35 hours the counts rate began to decrease because the generated particles started to deposit. During the first 21 hours the effective dose rate estimated directly by the RaDoM is about 5 times lower than the effective dose rate calculated from the radon concentration, due to the low value of the equilibrium factor between the radon and its progeny (about 0.1 rather than 0.4) and the amount of dust inside the chamber. As soon as the incense begins to burn (hour 21) the effective dose rate estimated by the RaDoM reaches the value of the dose rate calculated from the radon concentration and then decreases when the generated particles start settling (after 35 hours). In figure 14, the error bars associated to the dose evaluation based on the radon concentration (red line) have been assessed from the concentration uncertainty as reported by the Alphaguard [20]. The error bars associated to the dose measured by the RaDoM include type A and type B uncertainties as described in section 3.1. The effective dose over 45 hours obtained by the RaDoM and from the radon concentration are 0.81 ± 0.037 mSv and 1.86 ± 012 mSv (type A uncertainties), respectively.

2018 JINST 13 P07030

Figure 13. Measurement set-up inside the radon chamber at the Politecnico of Milano: the two RaDoM detectors, the Alphaguard reference radon monitor and the incense used to produce the particulate.

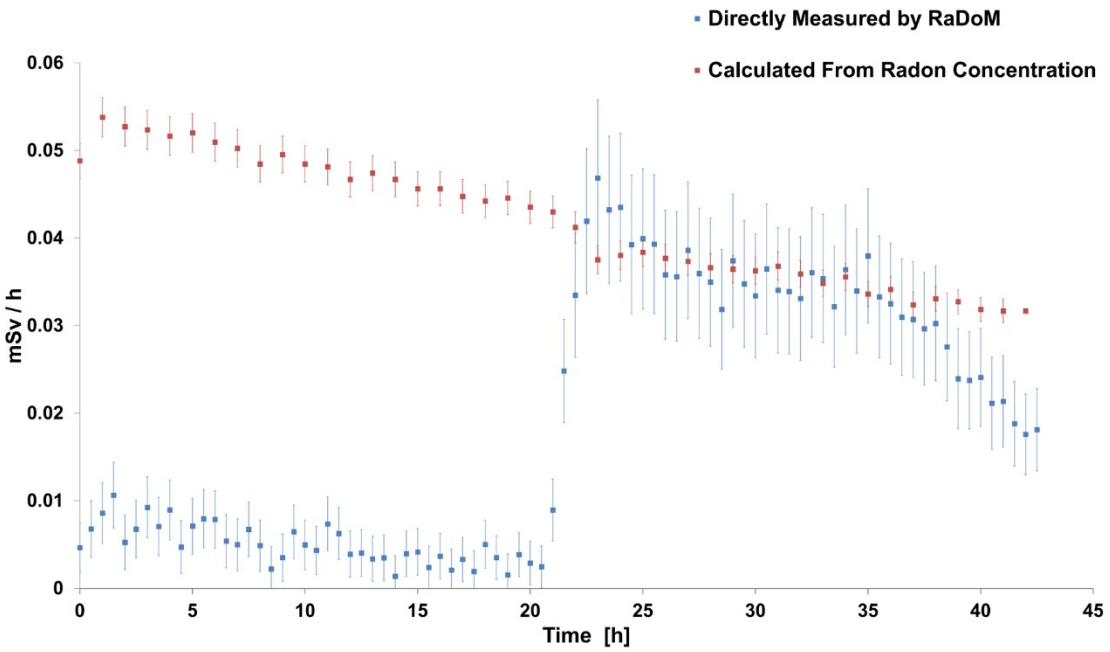

Figure 14. Effective dose rate measured directly with the RaDoM and calculated from the radon concentration assuming the standard equilibrium factor of 0.4.

2018 JINST 13 P07030

4 Conclusions

The first experimental results indicated that the RaDoM has a good capability of assessing the effective dose in situations where the environmental conditions are characterized by a standard equilibrium factor (F=0.4) and a standard unattached fraction of the PAEC (8%). On the other hand, in environments like the radon chamber characterized by a low equilibrium factor, the RadoM correctly assesses a lower effective dose with respect to the value calculated from the radon concentration. By changing the particulate concentration, the RaDoM response varies accordingly. The RaDoM has proved his capability to behave as a dosemeter with a response function that is reasonably independent of the concentration of the airborne particulate. It is worth underlining that the RaDoM can perform long-term measurements and can be useful in borderline situations where the radon concentration is close to the action level and a dose assessment can be needed. The RaDoM can also play a key role in situations where the equilibrium factor is expected to change during the measuring period [21]. Another feature of RaDoM is that it avoids the ^{210}Po contamination, which is a major problem with most active radon monitors like the ALPHAGUARD, as well as in RADONPIX and RADONLITE. In RaDoM the radon decay products attach to the filter surface, which can be easily replaced, rather than to the detector. However the problem recurs partially when the particles are electrically charged, such as in generation by combustion, because they are attracted by the positive charge of the silicon sensor. By setting the aluminum filter drawer at the same potential as the silicon sensor the contamination problem will be fully resolved. Future improvements of the dosimeter entails the replacement of the Timepix by a single silicon diode. This reduces the manufacturing cost of the detector. By using a silicon diode it is also possible to build a stand-alone device, integrating a microcontroller and a display unit, thus overcoming the need of a computer connected to the detector.

References

[1] UNSCEAR, *Effects of ionizing radiation, sources-to-effects assessment for radon in homes and workplaces*, UNSCEAR 2006, Report to the general assembly (Annex E).

[2] World Health Organization, *Who handbook on indoor radon: a public health perspective*, 2009.

[3] ICRU Report 88, *Measurement and Reporting of Radon Exposures*, December 2015.

[4] UNSCEAR, *Sources and effects of ionizing radiation*, United Nations University Press (2000).

[5] M. Caresana, L. Garlati, F. Murtas, S. Romano, C.T. Severino and M. Silari, *Real-time measurements of radon activity with the Timepix-based RADONLITE and RADONPIX detectors*, 2014 *JINST* **9** P11023.

[6] M. Campbell, *10 years of the Medipix2 Collaboration*, *Nucl. Instrum. Meth.* **A 633** (2011) S1.

[7] T.T.K. Cheung, K.N. Yu and D. Nikezic, *Bronchial dosimeter for radon progeny*, *Appl. Radiat. Isotopes* **55** (2001) 707.

[8] I. Takeshi, F. Kenzo, T. Shinji and K. Ryuhei, *Characteristics of major filters used for ^{222}Rn progeny measurements*, *Radiat. Meas.* **29** (1998) 161.

[9] https://www.knf.com/products/oem-pumps/product/products/diaphragm-gas-pumps/micro-pumps/.

2018 JINST 13 P07030

[10] R. Tykca and J. Sabol, *Low level environmental radioactivity*, TECHNOMIC publishing co.inc. (1995).

[11] P. Morrow, D. Bates, B. Fish, T. Hatch and T. Mercer, *Deposition and retention models for internal dosimetry of the human respiratory tract*, *Health Phys.* **12** (1966) 173.

[12] https://github.com/joelvogt/.

[13] D. Turecek, T. Holy, J. Jakubek, S. Pospisil and Z. Vykydal, *Pixelman: a multi-platform data acquisition and processing software package for Medipix2, Timepix and Medipix3 detectors*, 2011 *JINST* **6** C01046.

[14] https://www.scipy.org/.

[15] https://root.cern.ch/.

[16] M. Brugger, P. Carbonez, F. Pozzi, M. Silari and H. Vincke, *New radiation protection calibration facility at CERN*, *Radiat. Prot. Dosim.* **161** (2013) 181.

[17] P.K. Hopke, M. Ramamurthi and E.O. Knutson, *A measurement system for rn decay product lung deposition based on respiratory models*, *Health Phys.* **58** (1990) 291.

[18] ICRP, *Protection against radon-222 at Home and at work*, ICRP Publication 65, *Ann. ICRP* **23** (1993).

[19] ICRP, *The 2007 recommendations of the International Commission on Radiological Protection*, ICRP Publication 103, Pergamon Press, Oxford (2007).

[20] https://www.bertin-instruments.com/product/radon-professional-monitoring/radon-alphaguard/.

[21] T. Iimoto, *Time variation of the radon equilibrium factor in a reinforced concrete dwelling*, *Radiat. Prot. Dosim.* **92** (2000) 319.

2018 JINST 13 P07030